PHYSICAL REVIEW B VOLUME 20, NUMBER 8 15 OCTOBER 1979

Study of plasmon–LO-phonon coupling in Te-doped $Ga_{1-x}Al_xAs$

O. K. Kim and W. G. Spitzer

Departments of Physics and Materials Science, University of Southern California, Los Angeles, California 90007

(Received 28 March 1979)

Plasmon–LO-phonon coupling in n-type $Ga_{1-x}Al_xAs$ has been investigated by measuring the infrared reflectivity spectra of differently doped n-type samples having $x \simeq 0.14$, $x \simeq 0.30$, and $x \simeq 0.46$. Two expressions for the dielectric function, one an additive form and the other a factorized form, have given satisfactory fits to the reflectivity data. The mode frequencies and damping rates in the plasmon–LO-phonon coupled mode systems are calculated and compared with the observed ones for the samples having $x \simeq 0.14$ and $x \simeq 0.46$. The Γ-point conduction-band effective mass for $x \simeq 0.14$ is found to be $m^*_\Gamma = (0.13 \pm 0.01)m_e$ and the resistivity obtained from the infrared spectra is approximately 30% higher than the value from dc measurements. The reflectivity minima are broadened by the large plasma damping in the samples having $x \simeq 0.46$.

I. INTRODUCTION

$Ga_{1-x}Al_xAs$ is a mixed III-V compound semiconductor material which has been of technological importance during the last decade because of its application in light-emitting diodes and semiconductor lasers. It is also an alloy system of considerable intrinsic interest and has been the subject of numerous studies. It is therefore somewhat surprising that studies of plasmon-phonon interactions have not been reported since an understanding of this subject is of significant importance.

When free carriers are present in polar semiconductors, the collective excitations of carriers (plasmons) couple with longitudinal-optical (LO) phonons via the electric fields. These coupled-mode systems have been examined theoretically by Varga[1] and by Singwi and Tosi,[2] and experimentally by many investigators in a number of polar semiconductors such as GaAs,[3,5] GaP,[6,7] CdTe,[4,8] and CdS.[7,9] Although some infrared studies have been reported for the II-VI compound semiconductor alloy systems,[10,11] there have been no investigations of plasmon-phonon coupling in $Ga_{1-x}Al_xAs$ or, for that matter, in any of the pseudobinary III-V compound semiconductor alloys. The $Ga_{1-x}Al_xAs$ system is of particular interest since it is an example of the coupling phenomenon in a material having "two-mode" behavior.[12] In a two-mode system one observes two transverse-optical (TO) phonon frequencies which occur at frequencies close to those of the end members, i. e., $x = 0$ and $x = 1$, with the strength of each mode dependent on the fraction of each component present in the alloy. In the reststrahlen band region the reflectivity spectrum of undoped $Ga_{1-x}Al_xAs$ shows a clean two-mode behavior.[13] Most two-mode systems have some additional weak structure. The origin of this weak structure is not well understood. Therefore, the $Ga_{1-x}Al_xAs$ alloy is an attractive, relatively uncomplicated system in which to study plasmon-phonon coupling.

In the present study plasmon–LO–phonon coupled modes in Te-doped $Ga_{1-x}Al_xAs$ crystals have been investigated with infrared reflectivity measurements. The energy-band structure varies with alloy composition from a direct band gap for $x \lesssim 0.37$ to an indirect band gap for $x \gtrsim 0.37$.[14] Therefore, three different compositions were chosen, one in the direct-band-gap region, one in the indirect-band-gap region, and the third near the direct-indirect band-gap crossover point. The analysis of the reflectivity spectra is emphasized for the first two compositions. In the third case, where $x \simeq 0.30$ and the material is strongly n type, free electrons are present in significant concentrations in the conduction-band minima at the Γ, L, and X points. The different electron effective masses cannot be meaningfully distinguished by a direct interpretation of the reflectivity spectra.

In the analysis of the reflectivity spectra two different expressions have been used to represent the dielectric dispersion. One is a conventional additive form for the dielectric function in which ϵ is expressed as the sum of lattice terms and "Drude-like" free-carrier terms. The other expression is a factorized form ϵ_f,[5] from which the frequencies and damping rates of coupled modes can be readily found. Both expressions have given satisfactory fits to reflectivity data and have yielded reasonable values for the carrier concentration in several semiconductor systems.[4] The validity of both forms was demonstrated for undoped $Ga_{1-x}Al_xAs$ in a prior study.[13]

 © 1979 The American Physical Society

II. EXPERIMENTAL

A. Samples

The $Ga_{1-x}Al_xAs$ samples used in this study were grown by using an isothermal liquid-phase epitaxial (LPE) technique.[13] The melts were maintained in a small vertical temperature gradient with the substrates at the bottom and with excess GaAs and Al source floating on the upper surface. This method has been used to provide thick layers with good compositional uniformity. The substrates for the (LPE) layers were (100)-oriented wafers of Cr-doped or Te-doped GaAs. The Te dopant was introduced into the melt. The composition, x, and its variation with depth into the $Ga_{1-x}Al_xAs$ layers were evaluated by an ARL model EMX-SM electron-probe microanalyzer. The results indicated that the $Ga_{1-x}Al_xAs$ layer uniformity was $\Delta x \lesssim 0.02$ over a depth up to 150 μm from the interface between the substrate and the beginning of the $Ga_{1-x}Al_xAs$ layer. The thickness of the layers were generally greater than 150 μm although not uniform across the surface. Details concerning the growth method and the quality of the LPE layers have been discussed elsewhere.[13]

The samples for the infrared reflectivity measurements were cut from the thick part of the LPE layers. The substrate was removed by lapping. The first grown surface was then polished with 0.3 μm alumina (Linde A) followed by chemical polishing with Mirrolite solution.[13] The last grown side of the LPE layer was lapped until the layer thickness was $\simeq 150$ μm. A coarse grit, 320 SiC powder, was used for the lapping to prevent multiple-reflection contributions from the back surface in spectral regions of transparency.

After the reflectivity measurement, Hall data were measured by using the Van der Pauw method. The values of n_H in Table I were obtained by assuming a Hall scattering factor of unity so $R = -1/n_H e$. Ohmic contacts were prepared by using Au-12-wt %-Ge alloy.

B. Infrared reflectivity measurement

The infrared reflectivity data were taken point by point with a Perkin-Elmer B210 single-beam grating spectrometer in the frequency range from 240 to 780 cm^{-1}. The samples and a front-surface Al mirror were mounted on a sliding holder with the beam incident at nearly normal incidence, i.e., within approximately a 10° angle of incidence. The reflectivity was obtained by assuming a reflection of 98% for the Al mirror.[16] The spectral resolution varied but did not exceed 1.5 cm^{-1} in the frequency range $500 \gtrsim \omega \gtrsim 240$ cm^{-1}. The reflectivity spectra in the lower frequency range of $250 \gtrsim \omega \gtrsim 50$ cm^{-1} were measured with a Perkin-Elmer Model No. 180 far-infrared spectrometer equipped with two reflectance attachments. The spectral resolution was approximately 4 cm^{-1} for these measurements. The far-infrared reflectivity measurements were not sufficiently accurate to permit quantitative analysis but still served as a valuable qualitative guide. In all cases continuous frequency scans were taken to ensure that no structure in the reflectivity ocurred between measured points.

III. THEORY

In this section two forms of the classical dielectric dispersion are described briefly in order to provide a basis for the subsequent discussion of the results. More extensive discussions are available in the literature.[1,15] The infrared reflectivity R of a system having the two-mode behavior can be

TABLE I. Results of Hall measurement at 300 °K. Here $n_H = -1/eR_H$ is assumed.

Sample group	Sample No.	x	n_H (10^{18} cm^{-3})	ρ (10^{-2} Ω cm)	μ_H (cm^2/V sec)
I	1	0.14	0.032	7.0	2750
	2	0.13	1.8	0.24	1440
	3	0.14	2.8	0.18	1220
	4	0.15	4.8	0.12	1060
II	5	0.30	0.0042	170	880
	6	0.31	0.88	1.5	470
	7	0.29	1.9	0.95	350
III	8	0.44	···	···	···
	9	0.46	1.2	6.8	80
	10	0.46	···	···	···
	11	0.47	3.0	2.3	90

modeled from

$$R=[(N-1)^2+K^2]/[(N+1)^2+K^2],$$

where $\epsilon=(N+jK)^2$ and the conventional additive form is used for the dielectric function ϵ,

$$\epsilon=\epsilon_\infty+\frac{4\pi\rho_1\omega_{t_1}^2}{\omega_{t_1}^2-\omega^2-j\gamma_1\omega}+\frac{4\pi\rho_2\omega_{t_2}^2}{\omega_{t_2}^2-\omega^2-j\gamma_2\omega}-\frac{\epsilon_\infty\omega_p^2}{\omega(\omega+j\gamma_p)}. \quad (1)$$

Here N and K are the usual optical constants, ϵ_∞ is the high-frequency dielectric constant, ω_{t_i} the resonance frequency of lattice vibration, $4\pi\rho_i$ the oscillator strength, and γ_i the lattice phonon damping constant. The subscripts 1 and 2 are the GaAs-like and AlAs-like modes, respectively. The plasma frequency ω_p is defined by

$$\omega_p^2=\frac{4\pi ne^2}{\epsilon_\infty m^*}, \quad (2)$$

where n is the free-carrier concentration and m^* is the effective mass of the free carriers. In previous work[8] it was not necessary to introduce an energy-dependent plasma damping γ_p. In the present case we also assume damping constants are frequency independent. The LO frequencies of the lattice phonons, $\omega_{\mathrm{LO}\,i}$, are obtained easily from the roots of the equation $\epsilon=0$ when $\omega_p=0$. With negligible phonon damping constants, the GaAs-like LO frequency $\omega_{\mathrm{LO}\,1}$ and the AlAs-like LO frequency $\omega_{\mathrm{LO}\,2}$ are determined for the equations given by

$$\omega_{\mathrm{LO}\,1}^2+\omega_{\mathrm{LO}\,2}^2=\left(1+\frac{4\pi\rho_1}{\epsilon_\infty}\right)\omega_{t_1}^2+\left(1+\frac{4\pi\rho_2}{\epsilon_\infty}\right)\omega_{t_2}^2 \quad (3)$$

and

$$\omega_{\mathrm{LO}\,1}^2\omega_{\mathrm{LO}\,2}^2=\left(1+\frac{4\pi\rho_1}{\epsilon_\infty}+\frac{4\pi\rho_2}{\epsilon_\infty}\right)\omega_{t_1}^2\omega_{t_2}^2. \quad (4)$$

Another approach to describe the dielectric dispersion was introduced by Berreman and Unterwald.[17] Without reference to a particular model, the factorized dielectric function ϵ_f is given by

$$\epsilon_f(\omega)=\epsilon_\infty\frac{(\omega^2-\omega_{\ell_1}^2+j\gamma_{\ell_1}\omega)(\omega^2-\omega_{\ell_2}^2+j\gamma_{\ell_2}\omega)(\omega^2-\omega_{\ell_3}^2+j\gamma_{\ell_3}\omega)}{\omega(\omega+j\gamma_p)(\omega^2-\omega_{t_1}^2+j\gamma_{t_1}\omega)(\omega^2-\omega_{t_2}^2+j\gamma_{t_2}\omega)}, \quad (5)$$

where ω_{ℓ_i} and γ_{ℓ_i} are the eigenfrequencies and damping constants of the plasmon–LO-phonon coupled modes. The other parameters have interpretations similar to those in ϵ. The ϵ_f expression gives the coupled-mode frequencies and damping rates directly, however, it does not provide any independent physical interpretation for some of the parameters. From $\epsilon_f=0$, the plasmon–LO-phonon coupled-mode frequencies and damping rates are given by

$$\Omega_{\ell_i}=(\omega_{\ell_i}^2-\tfrac{1}{4}\gamma_{\ell_i}^2)^{1/2} \quad (6)$$

and

$$\Gamma_{\ell_i}=-\tfrac{1}{2}\gamma_{\ell_i}. \quad (7)$$

The coupled-mode frequencies are also obtained from the roots of $\epsilon=0$, where $\omega_p\neq 0$ which in the absence of damping leads to the following equation:

$$(\omega^2-\omega_p^2)(\omega_{t_1}^2-\omega^2)(\omega_{t_2}^2-\omega^2)+\frac{4\pi\rho_1}{\epsilon_\infty}\omega^2(\omega_{t_2}^2-\omega^2)+\frac{4\pi\rho_2}{\epsilon_\infty}\omega^2(\omega_{t_1}^2-\omega^2)=0. \quad (8)$$

If both of the dielectric functions ϵ and ϵ_f are valid representations for the description of the same physical phenomena, then the roots of $\epsilon=0$ and the roots of $\epsilon_f=0$ must be identical. A comparison of Eq. (8) and the numerator of the Eq. (5) gives the relations

$$\omega_{\ell_1}^2\omega_{\ell_2}^2\omega_{\ell_3}^2=\omega_p^2\omega_{t_1}^2\omega_{t_2}^2, \quad (9)$$

$$\begin{aligned}\omega_{\ell_1}^2\omega_{\ell_2}^2+\omega_{\ell_2}^2\omega_{\ell_3}^2+\omega_{\ell_3}^2\omega_{\ell_1}^2&=\left(1+\frac{4\pi\rho_1}{\epsilon_\infty}+\frac{4\pi\rho_2}{\epsilon_\infty}\right)\omega_{t_1}^2\omega_{t_2}^2+\omega_p^2(\omega_{t_1}^2+\omega_{t_2}^2)\\&=\omega_{\mathrm{LO}\,1}^2\omega_{\mathrm{LO}\,2}^2+\omega_p^2(\omega_{t_1}^2+\omega_{t_2}^2),\end{aligned} \quad (10)$$

and

$$\begin{aligned}\omega_{\ell_1}^2+\omega_{\ell_2}^2+\omega_{\ell_3}^2&=\left(1+\frac{4\pi\rho_1}{\epsilon_\infty}\right)\omega_{t_1}^2+\left(1+\frac{4\pi\rho_2}{\epsilon_\infty}\right)\omega_{t_2}^2+\omega_p^2\\&=\omega_{\mathrm{LO}\,1}^2+\omega_{\mathrm{LO}\,2}^2+\omega_p^2.\end{aligned} \quad (11)$$

Equation (9) is an extended Lyddane-Sachs-Teller relation which is valid even when the damping rates differ significantly from zero.[15]

Since the states near the conduction-band minima of GaAs-AlAs alloy semiconductors may involve valleys from regions of the Brillouin zone that are not symmetrically equivalent, the carrier contribution to the dielectric constant can be complicated. As shown schematically in Fig. 1,[14,18,19] the Γ, L, X minima are all important in the vicinity of the direct-indirect crossover point. The conduction electrons are distributed between the three types of band minima with different effective masses and scattering times, and therefore

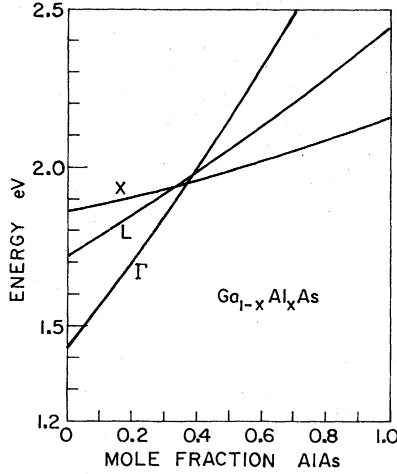

FIG. 1. Schematic diagram of band-gap energy at room temperature. The assumed conduction band edges were estimated from the values in Refs. 14, 18, and 19.

the dielectric function based on a "one-band" model should be modified. The free-carrier term, i.e., the last term in Eq. (1), can be replaced by

$$\epsilon_{fc} = -\epsilon_\infty \left(\frac{\omega_{p,\Gamma}^2}{\omega(\omega + j\gamma_{p,\Gamma})} + \frac{\omega_{p,X}^2}{\omega(\omega + j\gamma_{p,X})} + \frac{\omega_{p,L}^2}{\omega(\omega + j\gamma_{p,L})} \right). \quad (12)$$

Here

$$\omega_{p,\Gamma}^2 = \frac{4\pi n_\Gamma e^2}{\epsilon_\infty m_\Gamma^*}, \quad \omega_{p,L}^2 = \frac{4\pi n_L e^2}{\epsilon_\infty m_L^*}, \quad \omega_{p,X}^2 = \frac{4\pi n_X e^2}{\epsilon_\infty m_X^*}$$

and $\gamma_{p,\Gamma}$, $\gamma_{p,X}$, $\gamma_{p,L}$ are plasma damping constants related to Γ, X, L bands, respectively.

IV. RESULTS AND DATA ANALYSIS

A calculated R curve was fitted to the measured infrared reflectivity data points, $R_{i\,\text{expt}}$ by using ϵ given by Eq. (1) or by using ϵ_f given by Eq. (5). The fitting procedure made use of a computer program[20] which compared the experimental reflectivity with a computer calculated one until

$$\chi^2 = \frac{1}{M} \sum_{i=1}^{M} (R_{i\,\text{expt}} - R_{i\,\text{calc}})^2$$

was minimized, where M was the number of measured points. In one procedure Eq. (1) was used for the curve fitting with all of the parameters except ϵ_∞ allowed to vary for an independent determination. This procedure is hereafter called method (ia). A second procedure was one in which the independent variables in the fitting procedure were only ω_p and γ_p, and the parameters for the lattice vibrational terms and ϵ_∞ were fixed at the values previously determined[13] for the undoped samples. This procedure is called method (ib). In method (ib) it is assumed that the doping used to produce the carriers has negligible effect on the lattice phonon parameters. The correctness of this assumption has been verified for GaAs.[21] When Eq. (5) is used to obtain the best fit eigenfrequencies and damping constants of plasmon-LO coupled modes are determined directly. The ω_{ℓ_i}'s, γ_{ℓ_i}'s, ω_p and γ_p were varied to minimize χ^2, while ϵ_∞, ω_{t_i}'s and γ_{t_i}'s in the denominator of ϵ_f were fixed at the values obtained from the undoped samples, and this procedure is hereafter called method (ii). In each of the above methods the value of $\epsilon_\infty(x)$ was determined by using a linear assumption,

$$\epsilon_\infty(x) = (1-x)\epsilon_\infty(\text{GaAs}) + x\epsilon_\infty(\text{AlAs}), \quad (13)$$

where $\epsilon_\infty(\text{GaAs}) = 10.9$ and $\epsilon_\infty(\text{AlAs}) = 8.5$.

A. Samples with $x \simeq 0.14$

The $Ga_{1-x}Al_xAs$ samples with $x \simeq 0.14$ will be considered first, and as shown in Fig. 1 for this composition the Γ-point conduction-band minima is much lower in energy than the conduction-band minima at the X and L points. Therefore, the first term in Eq. (12) is the dominant one. The experimental reflectivity data points for this set of samples are shown in Fig. 2. The parameter val-

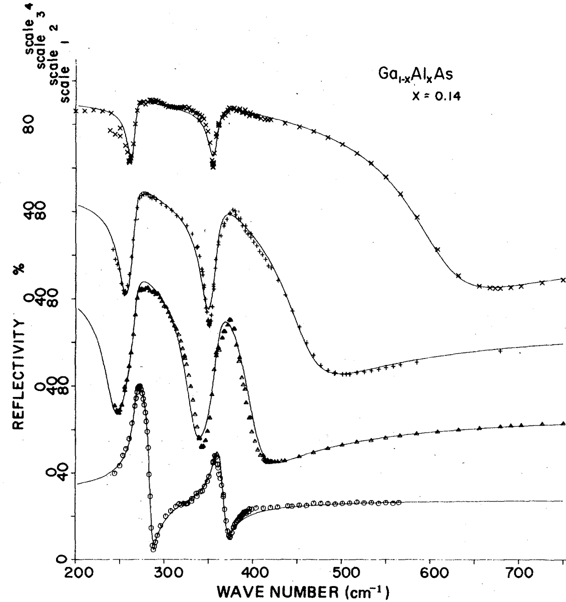

FIG. 2. Infrared reflectivity spectra of Te-doped $Ga_{1-x}Al_xAs$ having $x \simeq 0.14$. ○; indicate experimental data points for sample 1 by scale 1; Δ, sample 2 by scale 2; +, sample 3 by scale 3; and ×, sample 4 by scale 4. (——) are calculated curves by using the parameter values of method (ib) in Table II.

TABLE II. Parameters obtained from the curve-fitting procedure by using a conventional additive expression for a dielectric function. ω and γ in cm^{-1}.

Sample group	Sample No.	Method of analysis	ω_{t_1}	$\omega_{LO\,1}$	γ_1	ω_{t_2}	$\omega_{LO\,2}$	γ_2	ω_p	γ_p	$10^4\chi^2$
I	1	(ia)	267	286	5.2	359	369	9.0	⋯	⋯	3.97
	2	(ia)	267	284	7.9	359	367	8.9	347	53	3.97
		(ib)	267	286	5.2	359	369	9.0	343	60	8.05
($x \simeq 0.14$)	3	(ia)	267	287	6.6	359	369	7.1	429	79	5.06
		(ib)	267	286	5.2	359	369	9.0	430	77	9.33
	4	(ia)	268	295	7.3	359	369	6.4	601	102	2.03
		(ib)	267	285	5.2	359	370	9.0	602	96	4.95
II	5	(ia)	265	278	7.2	361	379	10.8	⋯	⋯	4.06
($x \simeq 0.30$)	6	(ib)	265	278	7.2	361	379	10.8	187	145	6.55
	7	(ib)	266	278	7.2	360	379	10.8	323	232	3.93
III	8	(ia)	263	273	7.6	360	386	9.6	⋯	⋯	3.82
	9	(ia)	263	272	10.0	361	385	10.4	140?	80?	1.74
		(ib)	263	272	7.6	361	386	9.0	130?	90?	5.90
($x \simeq 0.46$)	10	(ia)	⋯	⋯	⋯	⋯	⋯	⋯	⋯	⋯	⋯
		(ib)	263	272	7.6	361	386	9.0	170 ± 20	180 ± 50	6.57
	11	(ia)	264	274	9.0	362	384	10.0	260	314	2.23
		(ib)	262	271	7.6	361	386	9.0	269	389	12.8

ues listed in Table II were obtained by methods (ia) and (ib). In general, only slight differences between the two approaches were observed, primarily in the damping constants of the lattice vibration terms. The only exception is the GaAs-like LO frequency of sample 4 which showed a difference of ~ 10 cm^{-1}. As measured by χ^2, the fits were improved only by a factor of 2 by using method (ia) over method (ib) even though eight parameters were adjusted to minimize χ^2 in method (ia) while only two parameters were varied in method (ib). Reflectivity curves as calculated by using Eq. (1) with the parameter values obtained by method (ib) are plotted as solid lines in Fig. 2 for the samples of group I ($x \simeq 0.14$).

The parameter values obtained by method (ii) are listed in Table III. The quality of the best fit by this method as judged by minimizing the χ^2 values, is comparable to that by method (ia). The plasma frequencies ω_p were calculated by using Eq. (9) and they are essentially the same as those in Table II.

The normal-mode frequencies and damping rates of the plasmon–LO-phonon coupled-mode system are plotted as a function of plasma frequency in Fig. 3. They were obtained from Eq. (1) with $\epsilon = 0$ for two different plasma damping constants, i.e., $\gamma_p = 0$ and $\gamma_p = 80$ cm^{-1}. The lattice parameter values of the undoped sample and an assumption of negligible lattice damping rates were used in the

TABLE III. Parameters obtained from the curve-fitting procedure by using a factorized expression for a dielectric function; method (ii). ω and γ in cm^{-1}.

Sample group	Sample No.	ω_{l_1}	ω_{l_2}	ω_{l_3}	γ_{l_1}	γ_{l_2}	γ_{l_3}	γ_p	ω_p	$10^4\chi^2$	
I	2	244	337	402	23	22	25	79	345	4.78	$\omega_{t_1} = 267$
($x \simeq 0.14$)	3	254	348	466	17	14	58	82	430	5.25	$\omega_{t_2} = 359$
	4	261	355	623	13	12	88	100	600	2.63	$\epsilon_\infty = 10.57$
II	6	184	282	386	167	13	13	209	209	6.55	$\omega_{t_1} = 265$
($x \simeq 0.30$)	7	265	295	391	68	88	46	134	320	3.93	$\omega_{t_2} = 360.5$
											$\epsilon_\infty = 10.16$
III	9	120 ± 20	275	390	200 ± 40	18	11	270 ± 50	135 ± 20	3.37	$\omega_{t_1} = 263$
($x \simeq 0.46$)	10	145 ± 15	276	392	200 ± 40	13	16	270 ± 50	165 ± 15	3.96	$\omega_{t_2} = 360$
	11	245	275	390	190 ± 10	22	32	195 ± 10	278	3.57	$\epsilon_\infty = 9.80$

calculation. The real part, Ω_{ℓ_i}, and the imaginary part, Γ_{ℓ_i}, of a root of $\epsilon=0$ are the coupled-mode frequency and its damping rate. The plasma damping constant of $\gamma_p = 80\ \text{cm}^{-1}$ does not distort the coupled-mode frequencies significantly in most of plasma frequency range. The coupled-mode damping curves for the same γ_p show that in the plasma frequency range of $\omega_{\text{TO}_1} \lesssim \omega_p \lesssim \omega_{\text{LO}_2}$ the value of Γ_{ℓ_2} is substantial and there is the effect of the mixing of the three coupled modes. In the low-plasma-frequency range mode 1 is the plasmon-like and in the high-plasma-frequency range mode 3 becomes the plasmonlike mode. The values determined by the curve fitting, which utilized method (ii), for three samples in group I of Table III are also shown in Fig. 3. The coupled-mode frequencies agree well with the calculated ones and better agreement for Γ_{ℓ_i} is expected if we were to use a correct γ_p value for each sample instead of using the single value of $\gamma_p = 80\ \text{cm}^{-1}$.

The plasma frequency determined by the reflectivity and the measured Hall carrier concentration can be used to obtain the conduction-band effective mass. We can estimate the ratios between n_Γ, n_L, and n_X from an equation[22]

$$
\begin{aligned}
n_T &= n_\Gamma + n_L + n_X \\
&= A\left(\int_0^\infty \frac{(m^*_{D,\Gamma})^{3/2} E^{1/2}\, dE}{1+\exp[(E-E_F)/kT]} \right. \\
&\quad + \int_{\Delta E_L}^\infty \frac{(m^*_{D,L})^{3/2}(E-\Delta E_L)^{1/2}\, dE}{1+\exp[(E-E_F)/kT]} \\
&\quad \left. + \int_{\Delta E_X}^\infty \frac{(m^*_{D,X})^{3/2}(E-\Delta E_X)^{1/2}\, dE}{1+\exp[(E-E_F)/kT]} \right), \qquad (14)
\end{aligned}
$$

where $m^*_{D,i}$'s are the density-of-states effective masses of i conduction bands, E_F is the Fermi-energy level, ΔE_L and ΔE_X are energy separations of L and X minima with respect to Γ minimum, and $A = \sqrt{2}/\pi^2\hbar^3$. The n_L is estimated to be $\lesssim \frac{1}{3} n_\Gamma$ up to $E_F = \frac{2}{3}\Delta E_L$ by using the approximate values of $m^*_{D,\Gamma} \simeq 0.1\ m_e$, $m^*_{D,L} \simeq 0.88\ m_e$,[19] and the ΔE_L estimated from Fig. 1. From the energy separation of band energy levels it is apparent that $n_\Gamma > n_L > n_X$ at $x \simeq 0.14$, the R_H in this case is a three carrier expression for the multiple minima[19] and is given by

$$
R_H = -\frac{1}{e}\, \frac{n_\Gamma \mu_L^2 + n_L \mu_L^2 + n_X \mu_X^2}{(n_\Gamma \mu_\Gamma + n_L \mu_L + n_X \mu_X)^2}\ , \qquad (15)
$$

where μ_Γ, μ_L, and μ_X are mobilities of carriers in the respective minima. The mobility ratios μ_Γ/μ_L and μ_Γ/μ_X were assumed to be ~10 or more on the basis of a Hall data analysis by Kravchenko *et al.*[23] Therefore $R_H \simeq -1/en_\Gamma$. The n_Γ, n_L, and n_X estimated from Eq. (14) give neglibible values of $\omega^2_{p,L}$ and $\omega^2_{p,X}$ compared to $\omega^2_{p,\Gamma}$ and the

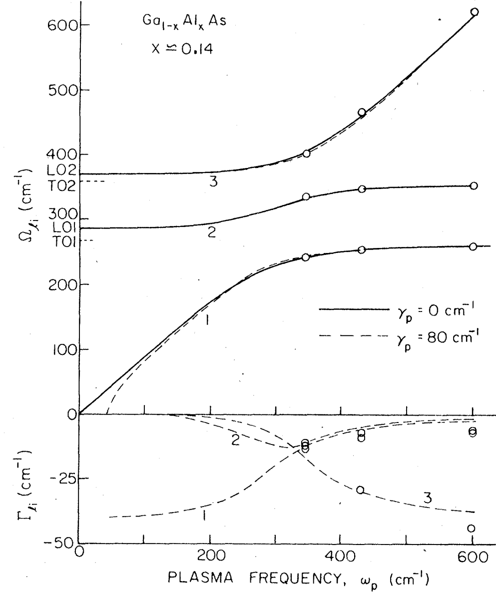

FIG. 3. Mode frequencies and damping rates in plasmon–LO-phonon coupled systems are plotted as a function of plasma frequence at $x \simeq 0.14$. (——) and (---) curves are calculated by assuming negligible lattice phonon damping and fixed values of γ_p. ○, experimental points.

expected large plasma damping constants also reduce the contribution of the second and third terms in Eq. (12) to the dielectric constant. Therefore, the second and third terms in Eq. (12) can be neglected, and thus we can give a reasonable estimate of the effective mass m^*_Γ from

$$
\omega_p^2 \simeq \omega^2_{p,\Gamma} = 4\pi n_\Gamma e^2/m^* \epsilon_\infty .
$$

By using the values of ω_p obtained from the curve fitting, we obtained $m^*_\Gamma = 0.13 m_e$ for samples 2 and 3, $m^*_\Gamma = 0.11 m_e$ for sample 4. A conservative estimation gives at most 10% error in m^*_Γ values of samples 2 and 3 due to the approximation used. The smaller effective mass for sample 4 could be the result of the fact that $n_L \simeq \frac{1}{3} n_\Gamma$ is not sufficiently small to be neglected. As a test of the analysis, Si-doped GaAs samples were carried through the same Hall and reflectivity measurements, and computer-program analysis as used for the $Ga_{1-x}Al_xAs$ samples. The effective mass of GaAs obtained from the above procedure, i.e., $m^*_{\text{GaAs}} = 0.091\ m_e$ for $n_H = 4.61\times 10^{18}\ \text{cm}^{-3}$ and $m^*_{\text{GaAs}} = 0.080\ m_e$ for $n_H = 1.17\times 10^{18}\ \text{cm}^{-3}$, agreed with the values in the literature.[24] These are masses ot the energy minimum at the Γ point and the change of m^*_Γ with n_H is due to nonparabolicity of the minumum. These m^*_Γ values are significantly smaller than those measured in the alloy samples with similar carrier densities.

To estimate m_Γ^* theoretically, a $\vec{k}\cdot\vec{p}$ perturbation theory[25,26] was used which considers the interaction of the Γ_1^c conduction band with the Γ_5^v valence bands and the Γ_5^c conduction bands. We also followed Berolo *et al.*[27] who assumed mixing of the valence and conduction-band states due to the alloy disorder in III-V alloy semiconductors. These theories predict a m_Γ^* dependent on x of $m_\Gamma^* \simeq m_{\text{GaAs}}^*(1+x)$ or less in the $Ga_{1-x}Al_xAs$ system. Considering both the x dependence of m_Γ^* on the degree of degeneracy,[28] the values $m_\Gamma^* = (0.13 \pm 0.01) m_e$ measured at $x \simeq 0.14$ for both samples 2 and 3 are larger by at least 20% than the theoretical estimates for the measured composition and carrier densities.

It is of interest to compare the optical resistivity given by $\rho_{ir} = 4\pi\gamma_p/\epsilon_\infty\omega_p^2$ with the measured dc value of ρ noting that ρ_{ir} is not explicity dependent on m^*. We have $\rho_{ir} \simeq 2.7 \times 10^{-3}$, 2.4×10^{-3}, and 1.6×10^{-3} Ω cm for samples 2, 3, and 4 by using the values of ω_p and γ_p of group I in Table II. The ρ_{ir} values are approximately 30% higher than the measured ρ values given in Table I, and the discrepancies might be due in part to our use of the Drude model which predicts an ω^{-2} dependence of free-carrier absorption coefficient or conductivity when $\omega \gg \gamma$. An ω^{-3} dependence[24] of the absorption coefficient in the high-frequency region ($\omega \gtrsim 500$ cm^{-1}) and ω^{-2} dependence[29] in the low-frequency region ($\omega \lesssim 200$ cm^{-1}) have been shown for GaAs. The ω^{-3} dependence of the absorption coefficient has been explained by a quantum model.[30]

B. Samples with $x \simeq 0.46$

For the samples of group III having the value of $x \simeq 0.46$ (see Table I) the lowest conduction-band minimum is located at the X point. Due to large conduction-band density of states, it is difficult to dope heavily this material enough to produce degenerate samples. For these samples the $\omega_{p,X}^2$ is the dominant contributor to the dielectric constant since $\omega_{p,L}^2$ and $\omega_{p,\Gamma}^2$ are small.

Unlike the samples with $x \simeq 0.14$, all samples in group III are nondegenerate and their experimental reflectivity data are shown in Fig. 4. The reflectivity minima are broadened as the carrier concentration increased. This effect is the result of high damping constants of the plasmon, i.e., low-electron mobilities. The lattice vibration parameters and free-carrier parameters in Tables II and III were obtained by following the curve fitting procedure described previously. The curves in Fig. 4 were calculated from ϵ with the parameter values obtained by method (ib), and the quality of the fits are comparable to those for the samples of group I. The lack of reliable reflectivity meas-

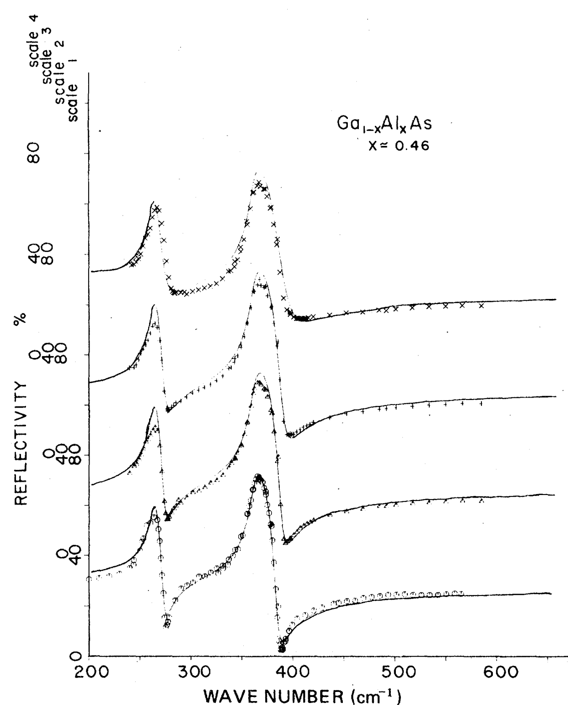

FIG. 4. Infrared reflectivity spectra of Te-doped $Ga_{1-x}Al_xAs$ having $x \simeq 0.46$. ○; indicate experimental data points for sample 8 by scale 1; Δ; sample 9 by scale 2; +; sample 10 by scale 3; and ×; sample 11 by scale 4. (——) are calculated curves by using the parameter values of method (ib) in Table II.

urements in the lowest frequency range, below 240 cm^{-1}, for samples 9 and 10, resulted in some significant uncertainties in the determination of ω_p and γ_p values by methods (ia) and (ib), and ω_{ℓ_1}, γ_p, and γ_{ℓ_1} values by method (ii). The free-carrier term in Eq. (1) hardly influence the reflectivity in the frequency range where $\omega_p^2/\omega^2 \ll 1$. Since ω_p of sample 9 is very low, i. e., $\omega_p^2/\omega^2 \ll 1$ in the region where the accurate reflectivity data are measured, the values of ω_p and γ_p for sample 9 determined by method (i) are not reliable. In method (ii) χ^2 values were very insensitive to the change of γ_p and γ_{ℓ_1} when the ratio γ_p/γ_{ℓ_1} was fixed, although χ^2 values increased rapidly from the minimum value as only one of the two parameters varied with all other parameter values fixed. For example, a 20% change in γ_p and γ_{ℓ_1} of samples 9 and 10 with the ratio γ_p/γ_{ℓ_1} held constant results in only a 5% increase in the χ^2 value, whereas the same change of γ_p with γ_{ℓ_1} and other parameters held fixed doubles the χ^2 value. The error ranges specified in Table III for the samples of group III are the values which induce approximately a 10% increase in the χ^2 value from the minimum. When a similar test was applied to the samples in group I, a slight variation of any parameter was not tolerable.

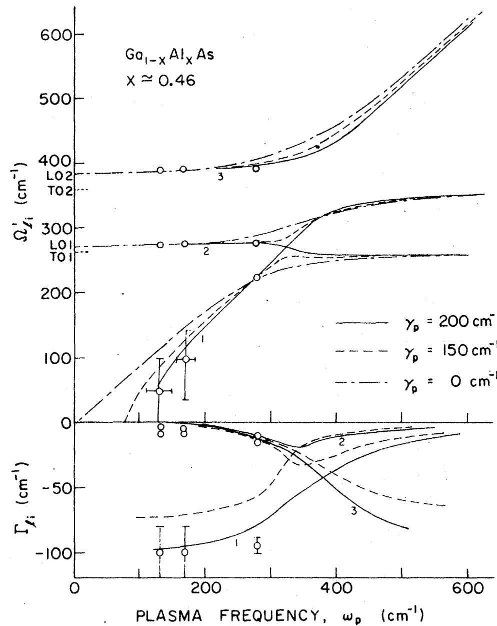

FIG. 5. Mode frequencies and damping rates in plasmon–LO-phonon coupled systems are plotted as a function of plasma frequency at $x \simeq 0.46$. The curves are calculated by assuming negligible lattice phonon damping and fixed values of γ_p. ○; experimental points.

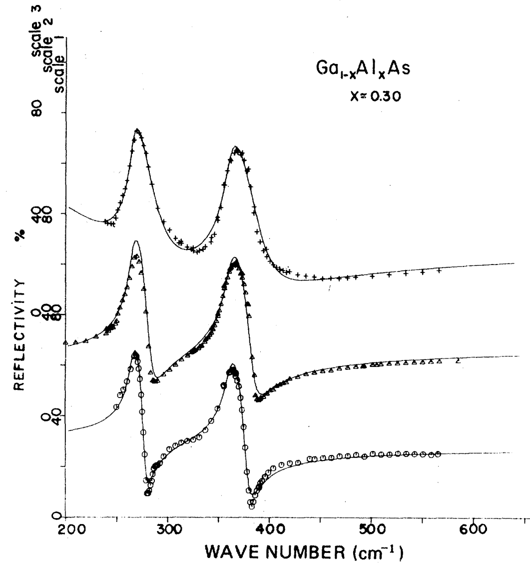

FIG. 6. Infrared reflectivity spectra of Te-doped $Ga_{1-x}Al_xAs$ having $x \simeq 0.30$. ○; indicate experimental data points for sample 5 by scale 1; Δ; sample 6 by scale 2; and +; sample 7 by scale 3. (——) are calculated curves by using the parameter values in Table II.

Coupled-mode frequencies and damping constants as a function of plasma frequency for $\chi \simeq 0.46$ are shown in Fig. 5. The frequencies (Ω_{ℓ_i}) and damping rates (Γ_{ℓ_i}) of coupled modes were calculated from zeros of the conventional additive form by assuming negligible damping of the lattice phonons and with several different plasmon damping constants, i.e., $\gamma_p = 0$, 150, and 200 cm⁻¹. Other lattice vibration parameters used in the calculation were the same as those of undoped material of the same composition. The calculated curves show that with $\gamma_p = 200$ cm⁻¹ ($\gamma_p \simeq 0.8\omega_{LO\,1}$) the mixing between plasma and GaAs-like LO phonon was weakened significantly, i.e., Ω_{ℓ_1} crossed over the GaAs-like TO frequency (TO 1) while for small plasma damping the Ω_{ℓ_1} approaches asymptotically this same TO frequency. The Γ_{ℓ_2} has relatively little change in the region of plasmon–LO–phonon coupling as shown in Fig. 5. Giehler and Jahne[7] show a similar calculation for CdS crystals, and they point out that the damping of the plasmons (as well as the phonons) counteracts the coupling in the region of $\omega_p \approx \omega_{LO}$. Experimental points determined by method (ii) and Eq. (9) are indicated with circles in Fig. 5 with error bars given because of the large uncertainties.

Our analyses show that both expressions for the dielectric constant give good fits to reflectivity data and that they provide comparable values of ω_p even though the plasma damping constants are large. Generally a large damping constant obscures the reflectivity minima and leads to difficulty in the determination of an accurate value for the plasma frequency. In spite of this fact, the estimated effective mass m_X^* from the plasma frequency observed for sample 11 is $m_X^* \simeq 0.4\,m_e$ which is comparable with the values $m_X^* \simeq 0.33\,m_e$ to 0.58 m_e given in the literature.[31] The m_X^* value obtained for sample 9 is ~$0.6 m_e$, however, the large error due to uncertainties in ω_p makes this value quite unreliable.

C. Samples with $x \simeq 0.30$

Since the energies of the conduction-band minima at Γ, X, and L points are comparable in $Ga_{1-x}Al_xAs$ when $x \simeq 0.30$, the free-carrier plasma contribution in each conduction band is treated as an independent excitation in the expression for the dielectric constant as given in Eq. (12). In principle one cannot find a meaningful interpretation of the data without knowing the scattering mechanism for the complicated band structure. If we assume the simple condition $\gamma_{p,\Gamma} = \gamma_{p,X} = \gamma_{p,L}$, then $\omega_p^2 = \omega_{p,\Gamma}^2 + \omega_{p,X}^2 + \omega_{p,L}^2$ is substituted in Eqs. (1) and (9). With this assumption we obtained the parameter values in Tables II and III for the samples in group II. The measured reflectivity data and the calculated reflectivity curves with the parameters obtained by method (ib) are shown in Fig. 6. The trend of

reflectivity and plasma damping have somewhat mixed results when compared to groups I and III. Similar to the result for the other composition the ϵ and ϵ_f yield essentially the same ω_p^2 by the curve-fitting procedures. We can roughly estimate ω_p values from Hall data by using Eqs. (14) and (15). These estimates agree with the values given in Tables II and III within approximately 30% when all plasma damping constants are assumed to be the same.

ACKNOWLEDGMENTS

This work was supported by Joint Services Electronics Program monitored by Air Force Office of Scientific Research under Contract No. F44620-76C-0061. The authors would like to thank D. B. Wittry for useful discussions during electron microprobe analysis and G. Rossman of the California Institute of Technology for the use of the far-infrared spectrometer system.

[1]B. B. Varga, Phys. Rev. 137, A1896 (1965).
[2]K. S. Singwi and M. P. Tosi, Phys. Rev. 147, 658 (1966).
[3]C. G. Olson and D. W. Lynch, Phys. Rev. 177, 1231 (1969).
[4]S. Perkowitz and R. H. Thorland, Solid State Commun. 16, 1093 (1975).
[5]S. Katayama and K. Murase, J. Phys. Soc. Jpn. 42, 886 (1977).
[6]M. Hashimoto and I. Akasaki, Phys. Lett. 25A, 38 (1967).
[7]M. Geihler and E. Jahne, Phys. Status Solidi B 73, 503 (1976).
[8]S. Perkowitz and R. H. Thorland, Phys. Rev. B 9, 545 (1974).
[9]J. F. Scott, T. C. Damen, J. Ruvalds, and A. Zawadowski, Phys. Rev. B 3, 1295 (1971).
[10]G. Dionne, and J. C. Woolley, Phys. Rev. B 6, 3898 (1972).
[11]S. W. McKnight, P. M. Amirtharaj, and S. Perkowitz, Solid State Commun. 25, 357 (1978).
[12]See, for example, A. S. Barker, Jr., and A. J. Sievers, Rev. Mod. Phys. Suppl. 47, S1 (1975).
[13]O. K. Kim, and W. G. Spitzer, J. Appl. Phys. 50, 4362 (1979).
[14]B. Monemar, K. K. Shih, and G. D. Pettit, J. Appl. Phys. 47, 2604 (1976).
[15]A. A. Kukharskii, Sov. Phys. Solid State, 14, 1501 (1972); Solid State Commun. 13, 1761 (1973).
[16]H. E. Bennett, M. Silver, and E. J. Ashley, J. Opt. Soc. Am. 53, 1089 (1963).
[17]D. W. Berreman, and F. C. Unterwald, Phys. Rev. 174, 791 (1968).
[18]E. Hess, I. Topol, K. R. Schulze, H. Newmann, and K. Unger, Phys. Status Solidi B 55, 187 (1973), and references therein.
[19]D. E. Aspnes, Phys. Rev. B 14, 5331 (1976).
[20]A. Kahan, Physical Science Research Papers No. 537, AFCRL-TR-73-0122 (unpublished).
[21]R. T. Holm, J. W. Gibson, and E. D. Palik, J. Appl. Phys. 48, 212 (1977).
[22]R. A. Smith, *Semiconductors* (Cambridge U. P., Cambridge, England, 1959), pp. 22–37.
[23]A. F. Kravchenko, Y. E. Maronchuk, and N. A. Yakusheva, Phys. Status Solidi A 30, 543 (1975).
[24]W. G. Spitzer and J. M. Whelan, Phys. Rev. 114, 59 (1959).
[25]C. Hermann and C. Weisbuch, Phys. Rev. B 15, 823 (1977).
[26]D. J. Chadi, A. H. Clark, and R. D. Burnham, Phys. Rev. B 13, 4466 (1976).
[27]O. Berolo, J. C. Woolley, and J. A. Van Vechten, Phys. Rev. B 8, 3794 (1973).
[28]K. Okada and T. Oku, Jpn. J. Appl. Phys. 6, 276 (1967).
[29]S. Perkowitz, J. Phys. Chem. Solids 32, 2267 (1971).
[30]B. Jensen, Ann. Phys. (N.Y.) 95, 229 (1975).
[31]S. Kratzer and J. Frey, J. Appl. Phys. 49, 4064 (1978).